Focused Tomography: Reducing CT Radiation Exposure for Region of Interest Viewing

Stephanie Leon and Timothy Olson
Departments of Radiology and Mathematics
The University of Florida, Gainesville, FL

1 Introduction

Computerized Tomography (CT) has become a standard diagnostic tool in modern medicine. In the last 30 years, however, CT use has become so prevalent that the cumulative radiation dosage which patients are exposed to during their lifetime has increased dramatically [1]. The risk/reward tradeoffs for these diagnostic tools are hard to quantify. Often times a physician is only interested in a limited Region of Interest (ROI) which has been identified through clinical means or previous imaging. We believe that we can reduce the risk when a limited ROI is examined by significantly reducing the total radiation dosage. The reward of this imaging will be preserved, since the images of the ROI will be nearly identical to those achieved with full radiation dosage. Large radiation dosages are well known to be potential causes for cancer.

The original investigations into Region of Interest (ROI) tomography, called Local Tomography, did not return the actual density of the ROI [2]. Rather these returned an altered or transformed image which did preserve edges between varying tissues. We introduced Localized Tomography with the goal of returning the actual image of the ROI [3, 4]. This is possible when one realizes that the low frequency components of the image are the only components which need non-local x-rays for their estimation. The high frequency components can be measured with the local line integral measurements which pass through the ROI. Thus one does not need to send radiation on paths which don't intersect the ROI to find the high frequency components of the image. For an illustration of local versus non-local x-ray paths please review Figure 2.

Thus to provide a complete and accurate reconstruction of the ROI two methods were presented which featured a) Regular sampling of the x-rays through the ROI in order to reconstruct the high frequency components of the image, and b) Sparse sampling of the x-rays which do not intersect the ROI, allowing for the recovery of low frequency components of the image. The combination of these methods results in an accurate reconstruction of the ROI, with greatly reduced radiation dosages [3, 4].

Many other methods have been presented since these initial works. These methods work very well but only allow 0, 1 sampling, i.e. either an x-ray is measured along a line integral or it is not. This is not feasible with modern radar machinery.

We will concentrate in this proposal on a third method, which allows variable sampling of the x-rays. This will feature regular dosage radiation through the ROI, and dramatically reduced dosages through the portions of the body outside of the ROI. The lower dosage measurements outside of the ROI will be sufficient because they will only be utilized to determine the low-frequency components of the ROI image. Thus the lower signal to noise (SNR) measurements can be averaged producing adequate SNR measurements for these low frequency components. The detailed high-frequency components of the image will have standard SNR measurements. Thus the image in the ROI can be made arbitrarily close to that using complete radiation dosage, with dramatically lower dosages. We will propose simple methods to focus the tomographic imaging, while receiving an accurate image of the ROI.

The completion of this work will allow physicians to view and monitor Regions of Interest with radiation dosages which are 20% of the standard dosage. This work will augment, rather than compete with, efforts which primarily focus on improving receiver sensitivity.

2 Innovation

2.1 A Shift in Current Clinical Practice

Current clinical practice is to choose a body segment to be imaged, and expose the entire portion to the same radiation levels. Thus if the right shoulder is the Region of Interest, the entire chest from the neck to below the shoulder will be exposed to the same amount of radiation. We are proposing to allow the physician to ask for only an image of the left shoulder, or ROI. We will then concentrate radiation on that ROI, and use a greatly reduced amount of radiation on the rest of the upper chest cavity and neck. Similarly, when doing spinal imaging, the radiation will be concentrated on that portion of the spine which is of interest, minimizing the radiation elsewhere. This development will constitute a shift in clinical practice, which can eliminate up to 80% of the radiation dosage.

This may be especially meaningful concerning diagnostic endeavors with children and pregnant women. In this proposal we discuss the imaging of tissue structures in cylindrical volumes. The mathematical methods promise the possibility of imaging within formed structures that can directly follow the outline of the anatomy under concern.

There are many organs in the human body which are well known to be very susceptible to radiation exposure. The lungs are one such organ. *The lungs are also the number one cause of death due to cancer in the world.* Some of that is due to smoking, but increased radiation through the lungs will not minimize this risk. Similarly, many other organs, such as glands, ovaries, etc. are very susceptible to radiation exposure. Minimizing undo risk to these organs is the focus of this paper.

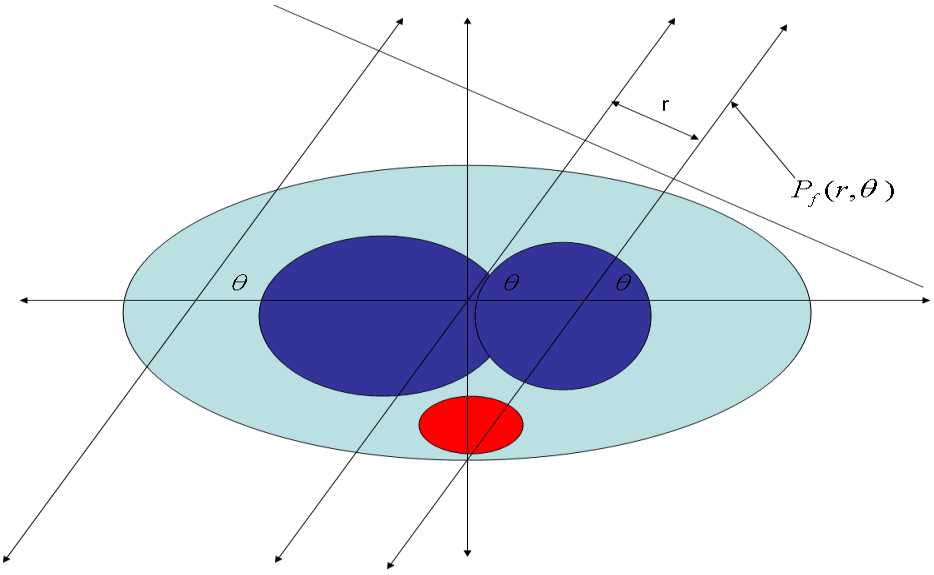

Figure 1: We illustrate the basics of the projection angles, coordinates, and vectors, r, θ, $\vec{\theta}$, and $\vec{x}$ above.

2.2 Novel Theoretical Concepts

We are able to accomplish this through a thorough understanding of the CT reconstruction process. CT data is generally collected in a helical fan-beam geometry. For the discussion of the reconstruction process it is easier if we assume that this data has been reformatted into a parallel beam data set. Thus we assume that the data can be viewed as a function of two variables, angle $\vec{\theta}$ and distance r from the origin, or that the data, which we refer to as the projections or sinogram, has the form

$$P_f(r,\vec{\theta}) = \int f(r\vec{\theta} + t\vec{\theta}^{\perp})dt.$$

This is illustrated in Figure 1

To this end, let us recall that the natural coordinates for tomography are $x = r\vec{\theta} + t\vec{\theta}^{\perp}$. Moreover $\vec{x} \cdot \vec{\theta}^{\perp} = r$. We want to see what the Fourier coefficients propagating at a fixed direction $\vec{\theta}$ have in common with the projections, so we consider

$$\hat{f}(s\vec{\theta}) = \frac{1}{2\pi} \int P_t(r,\vec{\theta}) e^{irs} dr. \tag{1}$$

Thus, a central slice of the two dimensional Fourier transform of $f(x,y)$, i.e. $\hat{f}(s\vec{\theta})$ can be obtained from the one dimensional projections of the function or $P_f(r,\vec{\theta})$. Formally stated, we have

Theorem 2.1 (Radon Transform, or Central Slice Theorem) *The one dimensional Fourier transform of $P_f(\vec{\theta}, r)$ is given by the central slice of the two dimensional Fourier transform, or $\hat{f}(s\vec{\theta})$. Mathematically,*

$$\mathcal{F}_1(P_f(r, \vec{\theta}) = \frac{1}{\sqrt{2\pi}} \hat{f}(s\vec{\theta}).$$

From this formula one can quickly derive the Filtered Backprojection formula, which was the basis of the 1979 Nobel prize.

$$\begin{aligned} f(\vec{x}) &\approx \frac{1}{2\pi} \int_0^{\pi} \int_{-\infty}^{\infty} \hat{f}(s\vec{\theta}) |s| w(s) e^{irs} ds d\theta \\ &= \int_0^{\pi} \left(P_f(r, \theta) * \mathcal{F}^{-1}(|s| w(s)) \right) (\vec{x} \cdot \vec{\theta}) d\theta. \end{aligned} \tag{2}$$

By choosing $w(s)$ appropriately we can make the approximation above arbitrarily small. If we denote $\mathcal{F}^{-1}(|s|w(s)) = k(r)$ then we have

$$f(\vec{x}) \approx \int_0^{\pi} \left(P_f(r, \theta) * k(r) \right) \right) (\vec{x} \cdot \vec{\theta}) d\theta, \tag{3}$$

where $*$ denotes convolution.

One problem with (3) is that the kernel $k(r)$ is very broad as a function of r, and as a result radiation measurements must be taken far from the Region of Interest. The reason for this kernel being broad is the jump discontinuity of the derivative of the function $|s|$ at the origin, from -1 to 1. Recall that $|s|$ is the necessary term due to the Polar coordinates used in the Fourier inversion of the Filtered Backprojection formula (2). The basic theorems of Fourier analysis dictate that this kernel cannot decay quickly.

We solve this problem by separating the discontinuity at the origin of $|s|$ into a separate portions $|s|w_2(s)$ at the origin, and $|s|(1 - w_2(s))$ away from the origin. The corresponding inverse Fourier transforms will the a low frequency kernel $k_l(r)$ which is the inverse Fourier transform of $|s|w_2(s)$, and a low frequency kernel $k_h(r)$ which is the inverse Fourier transform of $|s|(1 - w_2(s))$. This is illustrated in Figure 3. Thus we have $k(r) = k_l(r) + k_h(r)$. The filtered backprojection algorithm now looks like

$$f(\vec{x}) \approx \int_0^{\pi} \left(P_f(r, \theta) * k(r) \right) \right) (\vec{x} \cdot \vec{\theta}) d\theta, \tag{4}$$

$$= \int_0^{\pi} \left(P_f(r, \theta) * k_l(r) \right) (\vec{x} \cdot \vec{\theta}) d\theta + \int_0^{\pi} \left(P_f(r, \theta) * k_h(r) \right) \right) (\vec{x} \cdot \vec{\theta}) d\theta, \tag{5}$$

$$= f_l(\vec{x}) + f_h(\vec{x}). \tag{6}$$

Thus we will reconstruct the low and high frequency terms of $f(\vec{x})$ separately. The kernels are illustrated in Figure 4.

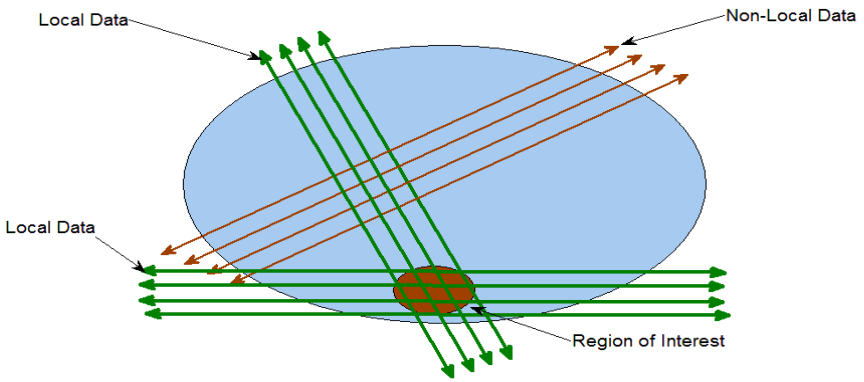

Figure 2: We illustrate the idea of the Region of Interest (ROI), local, and non-local data above. The Region of Interest (ROI), is in red, which might be an approximation for the spinal column of a patient. The green lines represent x-ray paths which pass through the ROI, and are therefore called local. The red lines represent x-ray paths which do not interest the ROI, and are therefore referred to as non-local. This project will minimize radiation along non-local x-ray paths.

Initially there seems to be no advantage to the change to two kernels $k_l(r)$ and $k_h(r)$ from a radiation reduction standpoint. The low frequency kernel will require the gathering of large quantities of data from outside the region of interest. Thus there is no apparent win in the fact that we can calculate the high frequency component $f_h(\vec{x})$ from completely local measurements.

One must understand the structure of the projections, and corresponding structure of the Filtered Backprojection algorithms to see how to solve our problems with the low frequency reconstruction $f_l(\vec{x})$. The structure theorem for the projections or Radon transform states that

$$P_f(\vec{\theta}, r) = (1 - r^2)^{-1/2} \sum_{l=0}^{\infty} T_l(r) h_l(\theta),$$

where $T_l(r)$ are the Chebyshev polynomials. Taking the Fourier transform of this yields

$$\begin{aligned} \hat{f}(s\vec{\theta}) &= \hat{P}_f(\theta, s) = (\frac{\pi}{2})^{-1/2} \sum_{l=0}^{\infty} i^{-1} J_l(s) h_l(\theta) && (7) \\ &= (\frac{\pi}{2})^{-1/2} \sum_{l=0}^{N-1} i^{-1} J_l(s) h_l(\theta) + (\frac{\pi}{2})^{-1/2} \sum_{l=N}^{\infty} i^{-1} J_l(s) h_l(\theta) && (8) \\ &= \hat{f}_l(s, \theta) + \hat{f}_h(s, \theta), && (9) \end{aligned}$$

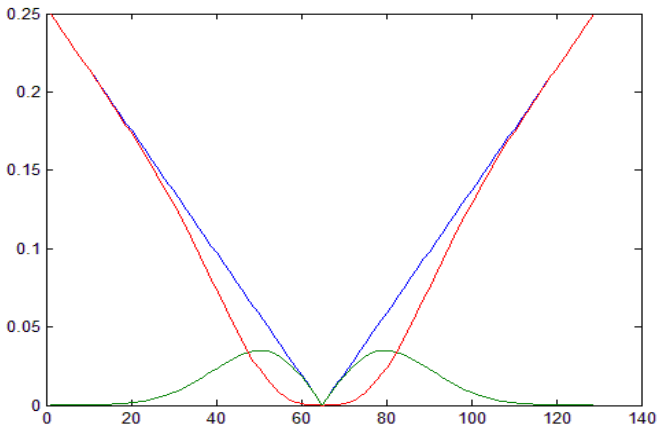

Figure 3: We show the correction term necessary for the inverse Fourier transform in Polar coordinates above, i.e. $|s|$. The problem with $|s|$ is the jump discontinuity at the origin of the derivative of $|s|$, from 1 to negative 1. This dictates that the inverse Fourier transform of $|s|w(s)$, even with a suitably smooth window $w(s)$ will be very wide, rather than narrow. This can be solved as above, with one "low frequency" term at the origin, and a "high frequency" term. The corresponding decomposition of the kernel $k_(r) = k_l(r) + k_h(r)$ will result in a low frequency kernel as a function of radius, $k_l(r)$, which is not locally supported, and a high frequency kernel $k_h(r)$ which is very narrow as a function of radius.

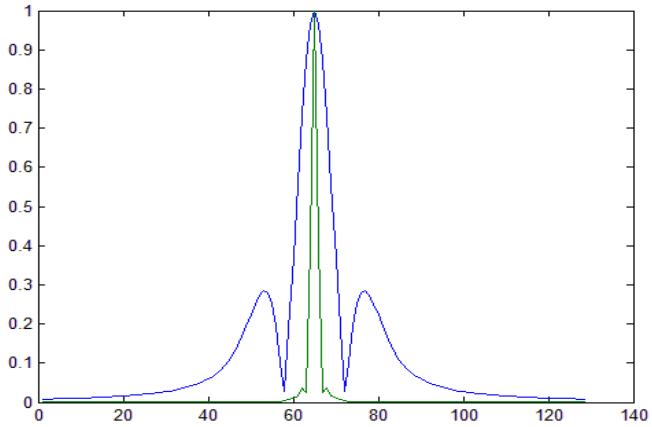

Figure 4: We show the kernel decompositions $k_l(r)$ and $k_h(r)$ above. The energy of $k_h(t)$ is contained within the interior 9 pixels of the current digitization or 9/512, to an accuracy of 1/10000. The energy concentration of $k_l(r)$, similarly measured, takes 175 terms. Thus the low frequency terms take a great deal of non-local information, and the high frequency terms can be measured locally.

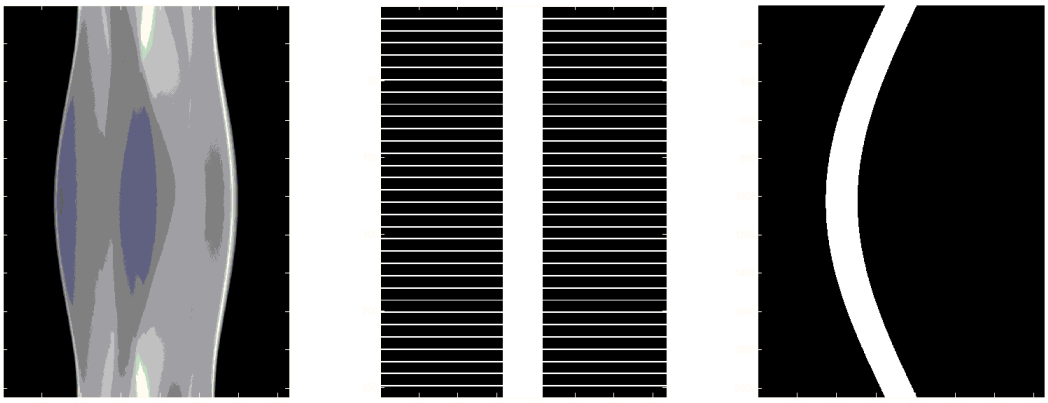

Figure 5: At the left we illustrate a standard Radon transform or sinogram. We illustrate the sampling recommended for a central region of an image in [3, 4] in the center. While this greatly reduced the radiation levels by as much as 90% was designed for parallel beam geometries, and not completely feasible for fan beam geometries. We illustrate the sampling which we are espousing for localized imaging in this project at the right. As opposed to the center sampling scheme, this is for an off-centered region. This will sampling scheme will also easily work with fan-beam Geometries.

where $J_l(s)$ are the Bessel functions, and $h_l(\theta)$ is an trigonometric polynomial of order l. The key to understanding (7) is that the low frequency terms in s, which are the Bessel functions, are only multiplied in frequency by the low order terms $h_l(\theta)$. Thus we do not have to measure the low frequency terms for many angles θ in order to accurately determine the complete low frequency components of the image.

This was the approach of Localized Tomography espoused in [3, 4]. The sampling of the Projections, or Radon transform is illustrated in Figure 5. This approach is not easily implemented on standard fan-beam CT machines, however. The sampling is 0-1, meaning that the x-ray tube would either have to be shut off or modulated very quickly to accomplish this type of sampling. Secondly, the sampling is based on a Parallel beam geometry. It is even more difficult to imagine this 0-1 sampling in this case.

2.3 Refinements and Improvements in Methodology and Instrumentation

We will now outline the refinements and improvements that will make this project feasible in a fan-beam geometry as well as a parallel beam geometry. The methods of [3, 4] and many of the subsequent follow-up papers by other authors concentrated on 0-1 sampling. Namely, a linear x-ray beam would be either sampled or not sampled. We will relax this condition,

and work to find the optimal solution to minimize radiation. Thus we will either sample at the necessary high-dosage rate, which is required for appropriate SNR and resolution in the ROI, or a variable lower-dosage rate, which is all that is necessary outside the ROI.

This optimal solution to this problem is necessarily better than the optimal solution to the 0-1 sampling problem. Any time more variables are added to an optimization problem, the solution necessarily gets better. Moreover, this will allow us to design the system in a way that is easily implementable in hardware. We can use static filters in front of the x-ray transmitter, to alter the beam for the appropriate reduced dosage.

We will now illustrate this approach, both mathematically and visually. It turns out that his approach is extremely simple both mathematically, and in implementation.

We will assume for now that the Region of Interest is circular, and for simplicity that the x-ray scanner is centered on the center of the circle when $\theta = 0$ (you can always do this). Then there is a distance d from the global center of the scanner to the center of the ROI, and we assume the ROI is a circle with radius r_1. As the gantry moves with θ the center of the circle will then be a distance $d(\theta) = d\sin(\theta)$ off of the center of the gantry. Thus we want to gather a full data set of the x-rays which pass through the ROI, which represent out first data set

$$P_f^h(\theta, r) = P_f(\theta, r),$$

where $0 \leq \theta \leq \pi$ and $r \in [d\sin(\theta) - r_1, d\sin(\theta) + r_1]$. This data set is gathered with full radiation dosage, just as if you were going to image the whole slice. There for it will have a relatively high SNR. The notation $P_f^h(\theta, r)$ recognizes that this data will be used to reconstruct the high frequency details of the image.

A second data set is then gathered from all of the lines or projections which did not intersect the region of interest. This is our low frequency data set

$$Pf^l(\theta, r) = P_f(\theta, r),$$

where $r \notin [d\sin(\theta) - r_1, d\sin(\theta) + r_1]$. This data set is gathered with minimal radiation, and will have very low SNR. This data will only be needed to reconstruct the low frequency portion of the image, however, and will not affect the final image in the ROI, however.

We now simply combine the data sets to get our approximate, noisy sinogram or Radon transform

$$P_f(\theta, r) \approx P_f^h(\theta, r) + P_f^l(\theta, r),$$

noting that we have sampled all of the Radon transform, some of it at high SNR and some at low SNR. Now our final reconstruction will be

$$\begin{aligned} f(\vec{x}) &\approx \int_0^\pi \left(P_f(r,\theta) * k(r)\right)\right) (\vec{x}\cdot\vec{\theta}) d\theta, \qquad (10) \\ &= \int_0^\pi \left(P_f(r,\theta) * k_h(r)\right) (\vec{x}\cdot\vec{\theta}) d\theta + \int_0^\pi \left(P_f(r,\theta) * k_l(r)\right)\right) (\vec{x}\cdot\vec{\theta}) d\theta \end{aligned}$$

$$= \int_0^\pi \left(P_f^h(r,\theta) * k_h(r) + P_f^l(r,\theta) * k_h(r)\right)(\vec{x}\cdot\vec{\theta})d\theta$$
$$+ \int_0^\pi \left(P_f^h(r,\theta) * k_l(r) + P_f^l(r,\theta) * k_l(r)\right)(\vec{x}\cdot\vec{\theta})d\theta.$$

We must now analyze these terms $P_f^h(r,\theta) * k_h(r)$ is the term which will yield most of our high resolution image, and is well sampled through the ROI. This is the foundation of our reconstruction. The second term $P_f^l(r,\theta) * k_h(r)$ will be essentially zero for any contribution to the ROI, since $P_f^l(r,\theta)$ is only sampled for lines that don't intersect the ROI, and $k_h(r)$ is extremely well localized as we commented in Figure 3. The term $P_f^h(r,\theta) * k_l(r)$ yield a high partial estimate for the low frequency components, while $P_f^l(r,\theta) * k_l(r)$ gives a rather low SNR estimate for the low frequency components.

Thus we have a very high SNR estimate for the high frequency components inside the ROI. We must recall the structure of the Radon transform to realize why the low frequency component is not affected by the low SNR estimates. Recall from (7) that the low frequency components are only affected by low frequency sines and cosines with respect to θ or that the Fourier transform

$$f_l(s\vec{\theta}) = \sum_{l=0}^{N-1} i^{-1} J_l(s) h_l(\theta).$$

Therefore we are estimating very few parameters in the low frequency component. We have a great number of data samples, so the law of large numbers will yield a very solid estimate for the low frequency component.

This process is illustrated in Figure 6. The original reconstruction and a noisier version are shown at the top. The second row shows the ROI reconstructed with a full data set, and with the reduced data set at right. The final row shows an off center ROI reconstructed from a large and small data sets. The radiation reduction was 92%.

A natural question might be "Do we really need to any data which doesn't pass through the ROI?"

3 Clinical Results

We obtained Institutional Review Board approval to acquire data by imaging a human cadaver at 4 different radiation dose levels: 2 milligray (mGy), 8 mGy, 18 mGy, and 60 mGy. To put perspective on this, most clinical abdominal CT scans reconstructed with filtered back-projection will use around 18-20 mGy for adults, with 60 mGy far exceeding the norm. Scanners using iterative reconstruction algorithms may use closer to 8 mGy for the same scan. For children or infants, lower doses such as 8 mGy or 2 mGy are routinely used. This is partially due to two reasons: 1) The much smaller body size, meaning its far easier to penetrate through the body, and 2) Increased attention to dose reduction, due to

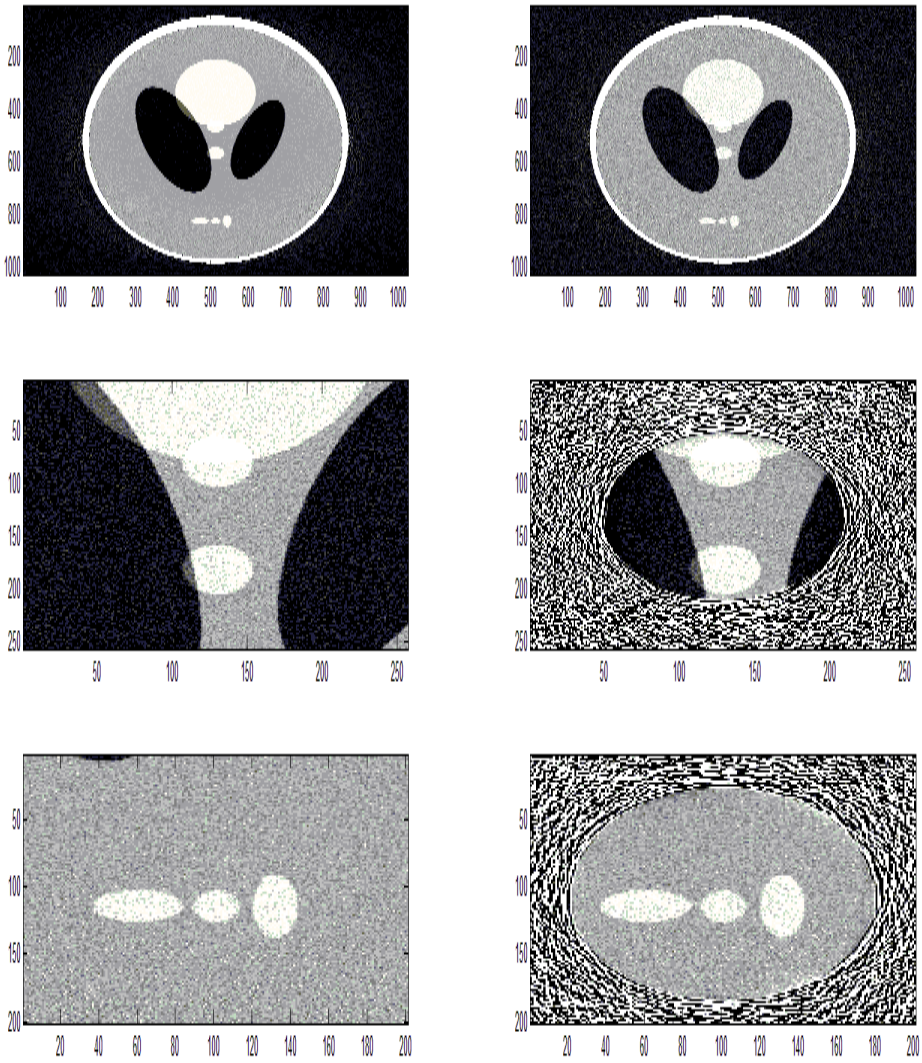

Figure 6: We illustrate the radiation exposure recommended for a central region and a non-central of an image similar to the schemes in [3, 4]. This results in a radiation levels by as much at least 92%. As opposed to the 0-1 sampling scheme in [3, 4], this adaptive sampling method was designed for arbitrary geometries, and an be implemented in a fan-beam geometry. The original non-noise related reconstruction is at top left, and a noisy reconstruction is at top left. The middle and bottom rows show the noisy reconstruction with full data on the left, and the reduced radiation reconstructions of a ROI on the right.

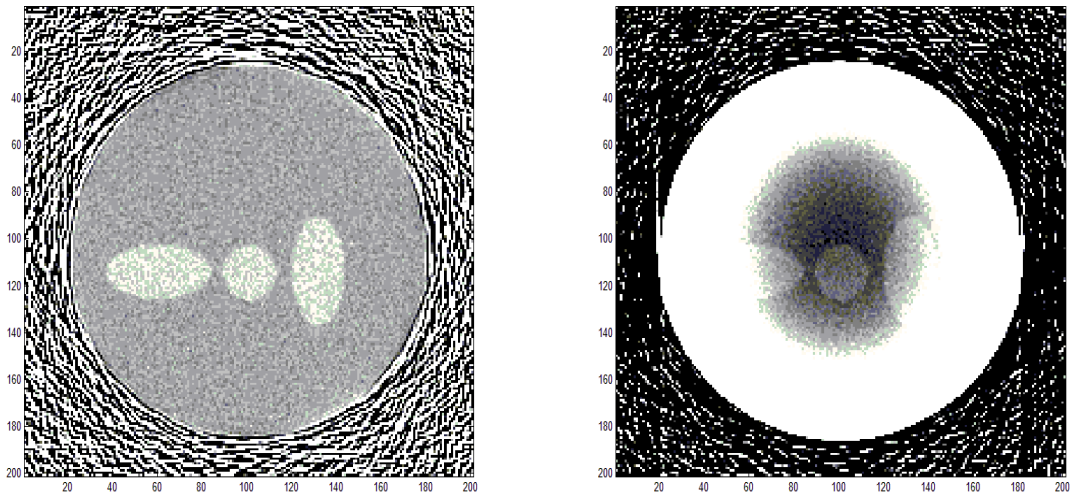

Figure 7: We illustrate a reconstruction from completely local data above. On the left is the localized reconstruction as was shown in Figure 6. The picture on the right is the reconstruction with totally local data, ignoring the steps for the localized data, Focused Tomography, as we outlined above. Obviously this is not desirable.

the higher radiosensitivity of children and the longer lifespan they have in which to develop a cancer with a long latent period.

The CT scanner we used did not permit further dose reduction below 2 mGy. Future clinical implementation of this technique will require the development of an adjustable collimator mechanism, which will allow us to reduce the ionizing radiation exposure to areas outside the area of focus to about 10

We have gathered data at 4 different dosage levels, 2mGy, 8mGy, 18mGy, and 60mGy. Understand that the mGy stands for milligray. To put perspective on this, the accepted clinical dosage level is 18-20mGy, with 60mGy far exceeding the normal. In addition, for children or infants, 8mGy or 2mGy might be used by the radiologist. This is partially due to two reasons: 1) The much smaller body size, meaning its far easier to penetrate through the body, and 2) The highly sensitive nature of using radiation on someone we hope will live another 70-80 years. Obviously the same concerns are present, but not as acute for someone in their 70's.

We would have gathered at levels well below 2mGy, but the scanner does not allow one to do that. Those levels are not seen as clinically viable. We used a Toshiba scanner for these measurements. Rather than altering scanners, we will use an attenuating focusing mechanism to obtain levels in the future which further minimize ionizing radiation exposure.

3.1 Clinical Pictures

We begin with two clinical pictures which illustrate our goals. We will stick with the measurements at 18mGy for the region of interest (ROI), and use use 2mGy for the exterior, non-ROI projections.

For simplicity we now specify two different modes for our images. We will denote the first by Focused Tomography 1 (FCT1) by which we use the lower dosage measurement outside the ROI and the higher dosage measurements inside the ROI with no transition region between them. We will denote the second by Focused Tomography 2 (FCT2) by which we have smooth windowed transition between the lower dosage and the higher dosage measurements.

The first clinical study is of a pelvis which is illustrated in Figure 8. The pelvis is crucial for a number of reasons. Pelvic injuries from car accidents or falls can become devastating, mobilization reducing injuries in both the young and old. For older patients, pelvic injuries from falls often times result in the loss of mobility. The loss of mobility and subsequent need for long term care will often times reduces quality of life and introduces extreme cost. In addition, it can result in a reduction of life expectancy, since the patient will not be able to do the basics of exercise, such as walking. Younger patients involved in a car or other accidents face similar and perhaps more dangerous problems. If a young woman is involved in a car accident, the necessity is to get her well and mobile. On the other hand the ovaries are critically exposed, and loss of reproductive health is certainly a large issue.

The second is of a spine which is illustrated in Figure 9. This is obviously a critical radiological measurement for many people. The spine is crucial for long term health, and is surrounded by organs which do not react well to ionizing radiation. A simple non-expansive list is: 1) The thyroid gland in the neck region, 2) The lungs, 3) The liver and pancreas, and 4) Vital reproductive organs in the pelvis. In addition, if surgery is done on the spine often times involving fusing two adjacent vertebrae, multiple CT scans will often be used for investigation and then evaluation of the fusing of the vertebrae.

In Figures 10 and 11 we illustrate that we can use even lower doses radiation outside the region of interest with nearly perfect results. There is a law of diminishing return in this and we believe that the radiation level is reduced by approximately 85% in these images. The images are of a spine with much lower dosage outside the ROI. We believe that this success is due to the low frequency coefficients being nearly invariant on standard human scans. We illustrate the same techniques in Figures 12 and 13 on a hip socket. Once again, remarkably perfect images of the ROI are retrieved with very low dosage.

The results of Figures 10-12 suggest that we can get away with far less off ROI radiation than a standard result would suggest. We believe that this is due to the low frequency component of human CT images being fairly invariant.

4 Engineering Implementation

We now illustrate in Figure 14 how we imagine that we will be implementing these radiation reduction techniques, in a modern scanner, for a very reasonable upgrade cost. As shown in Figure 14 we use a shielding mask, probably made from aluminum or a similar material, to reduce the radiation. The key is that the aluminum is selected at an appropriate thickness to allow some reduced dosage radiation to go through the non-ROI region. This aluminum mask will rotate to center on the main ROI, allowing full dosage radiation to be gathered from the ROI.

The non-ROI data will then be amplified artificially. This is why the non-ROI data will have much higher SNR levels.

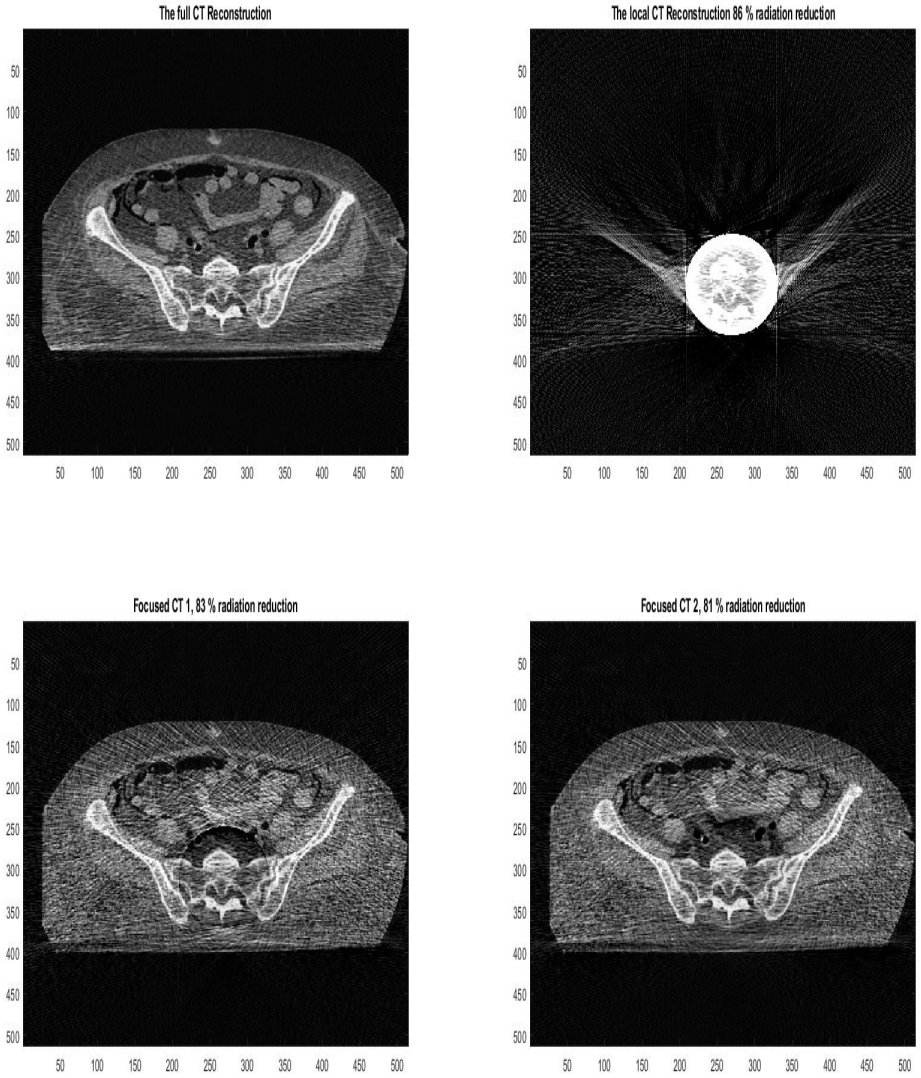

Figure 8: We illustrate the radiation exposure recommended for a central region and a non-central an Pelvic image similar to the schemes in [3, 4]. This results in a radiation levels by approximately 80%. As opposed to the 0-1 sampling scheme in [3, 4], this adaptive sampling method was designed for arbitrary geometries, and an be implemented in a fan-beam geometry. The original non-noise related reconstruction is at top left, the reconstruction with totally local data is seen on the right. The bottom row shows the reduced radiation methods with FCT1 on the left, and FCT2 on the right.

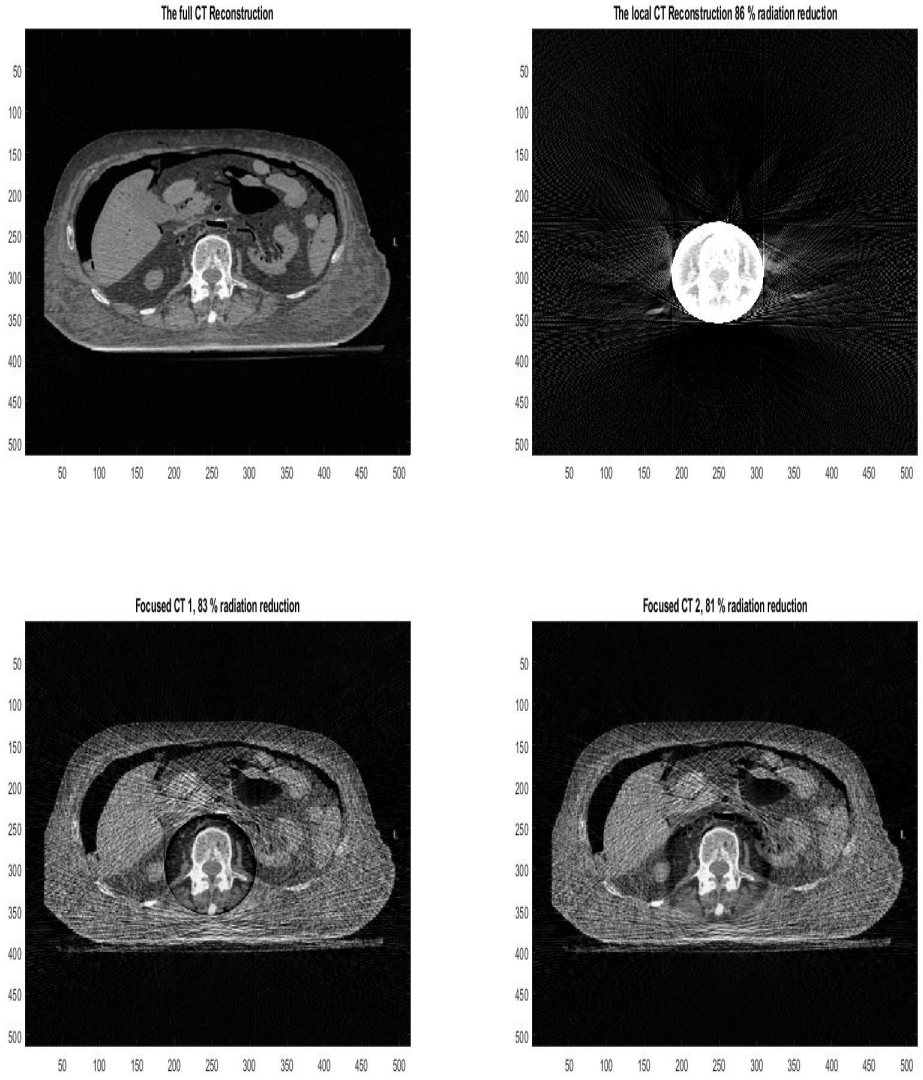

Figure 9: We illustrate the radiation exposure recommended for a central region and a non-central of an Spinal image similar to the schemes in [3, 4]. This results in a radiation levels by approximately 80%. As opposed to the 0-1 sampling scheme in [3, 4], this adaptive sampling method was designed for arbitrary geometries, and can be implemented simply in a fan-beam geometry. The original non-noise related reconstruction is at top left, the reconstruction with totally local data is seen on the right. The bottom row shows the reduced radiation methods with FCT1 on the left, and FCT2 on the right.

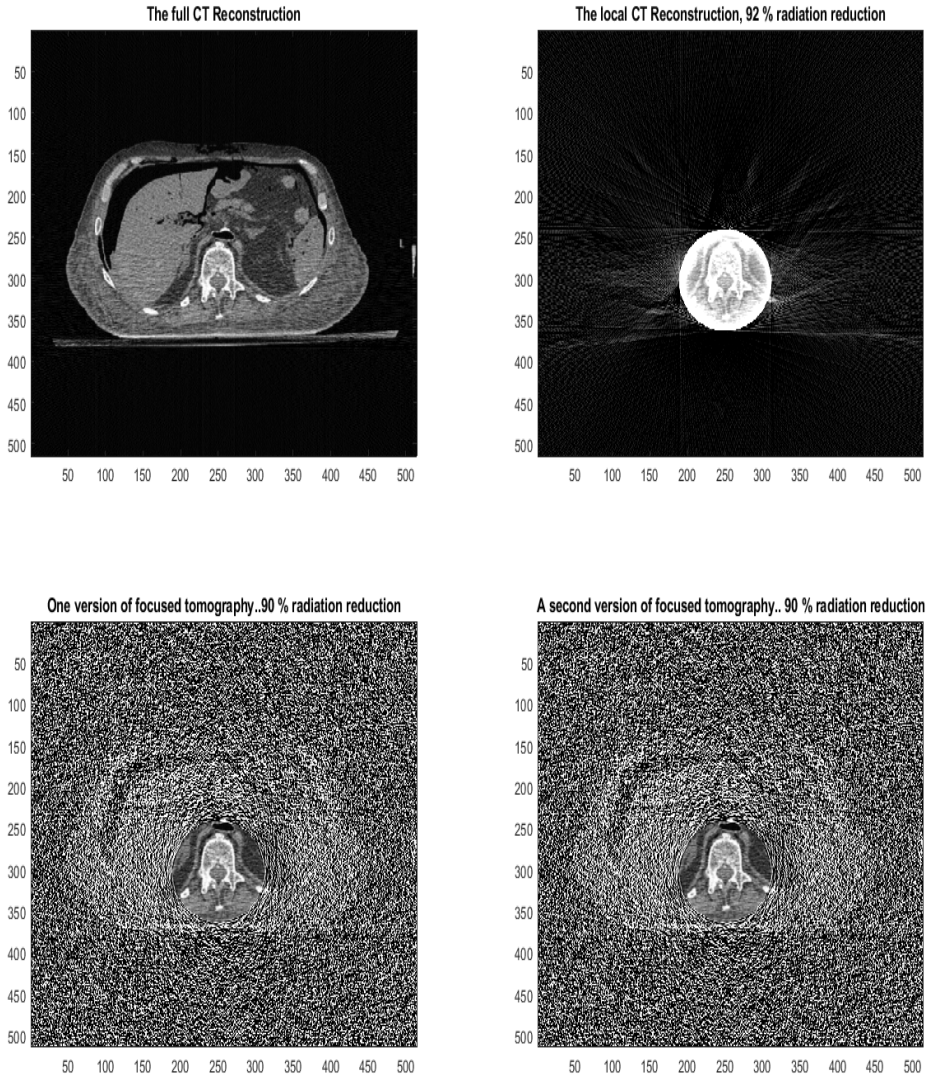

Figure 10: We illustrate the radiation exposure recommended for a central region and a non-central of an Spinal image similar to the schemes in [3, 4]. In these images we utilized off ROI radiation levels which were much lower than those of Figure 9. This results in a radiation levels by approximately 85%. As opposed to the 0-1 sampling scheme in [3, 4], this adaptive sampling method was designed for arbitrary geometries, and can be implemented simply in a fan-beam geometry. The original non-noise related reconstruction is at top left, the reconstruction with totally local data is seen on the right. The bottom row shows the reduced radiation methods with FCT1 on the left, and FCT2 on the right.

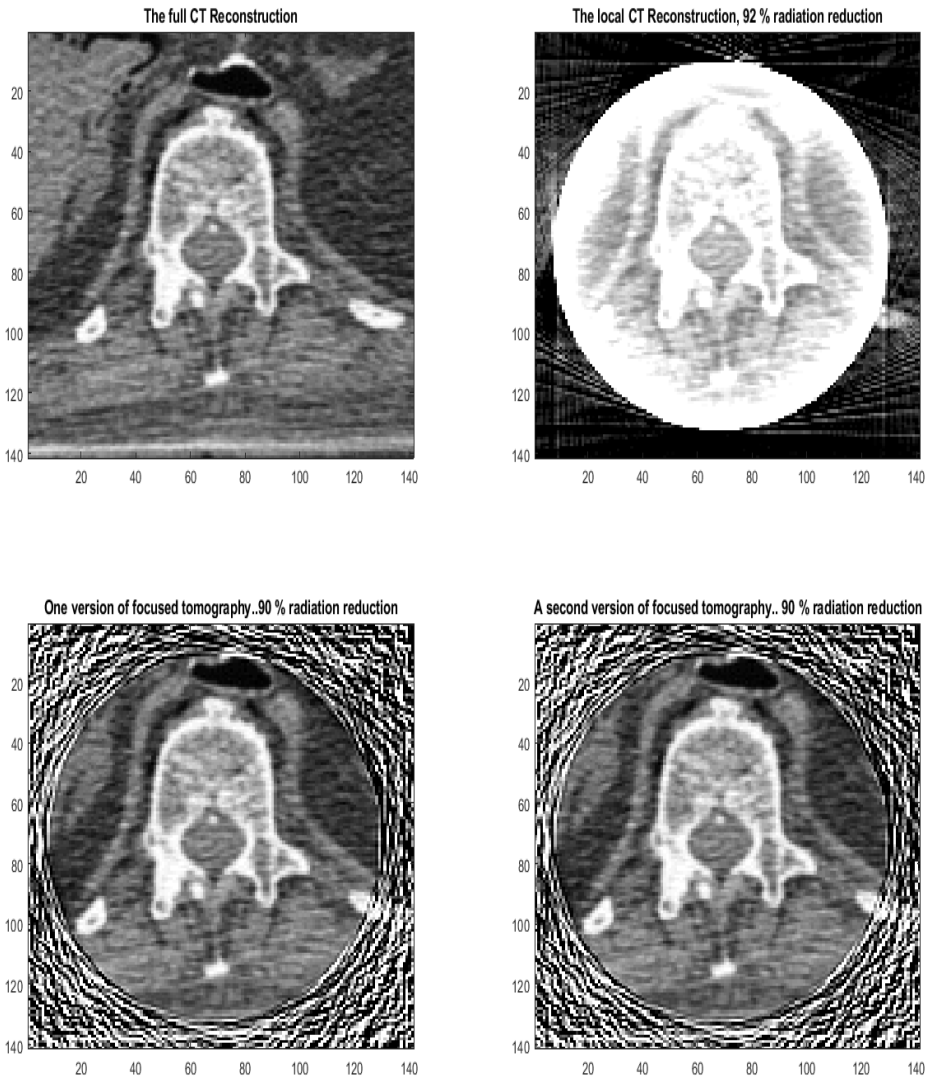

Figure 11: We illustrate the radiation exposure recommended for a central region and a non-central of an Spinal image similar to the schemes in [3, 4]. In these images we utilized off ROI radiation levels which were much lower than those of Figure 9. We illustrate closeups of the ROI above. This results in a radiation levels by approximately 85%. As opposed to the 0-1 sampling scheme in [3, 4], this adaptive sampling method was designed for arbitrary geometries, and can be implemented simply in a fan-beam geometry. The original non-noise related reconstruction is at top left, the reconstruction with totally local data is seen on the right. The bottom row shows the reduced radiation methods with FCT1 on the left, and FCT2 on the right.

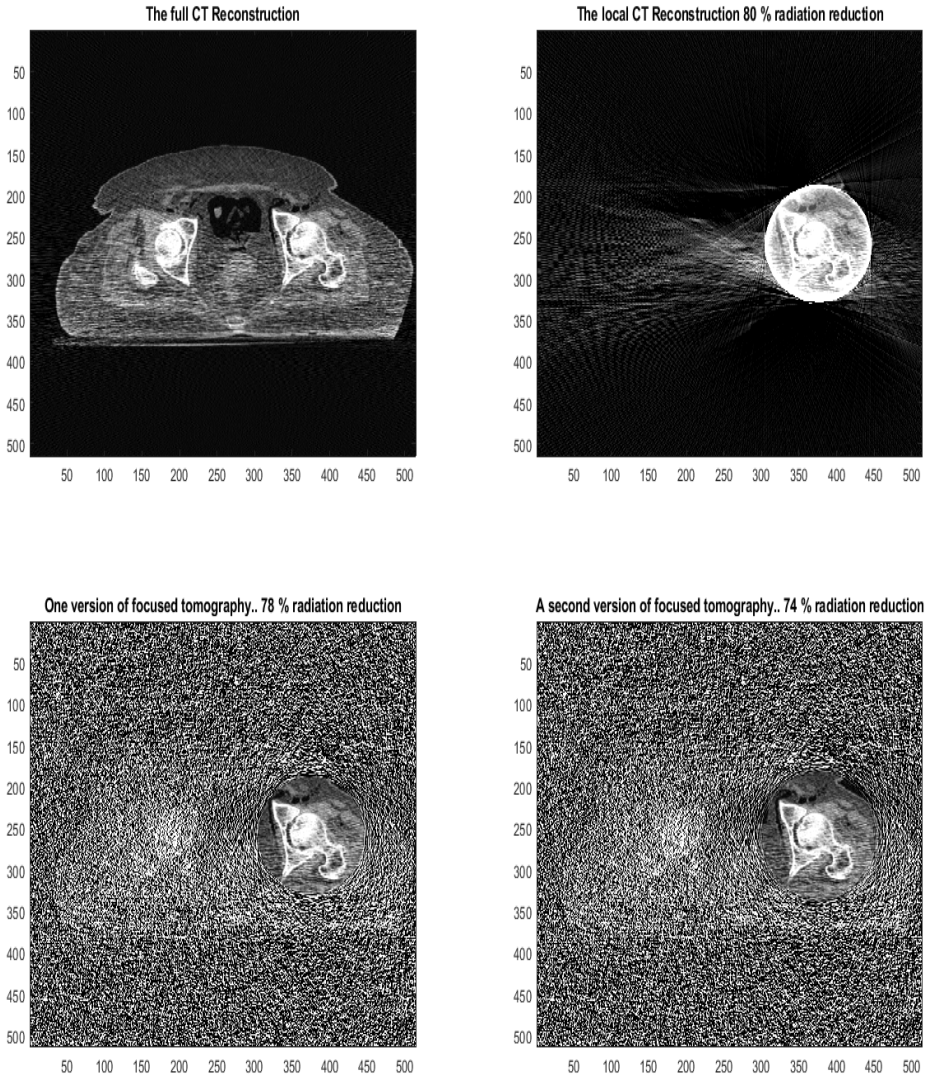

Figure 12: We illustrate the radiation exposure recommended for a central region and a non-central of an Hip socket image similar to the schemes in [3, 4]. In these images we utilized off ROI radiation levels which were much lower than those of Figure 9. This results in a radiation levels by approximately 85%. As opposed to the 0-1 sampling scheme in [3, 4], this adaptive sampling method was designed for arbitrary geometries, and can be implemented simply in a fan-beam geometry. The original non-noise related reconstruction is at top left, the reconstruction with totally local data is seen on the right. The bottom row shows the reduced radiation methods with FCT1 on the left, and FCT2 on the right.

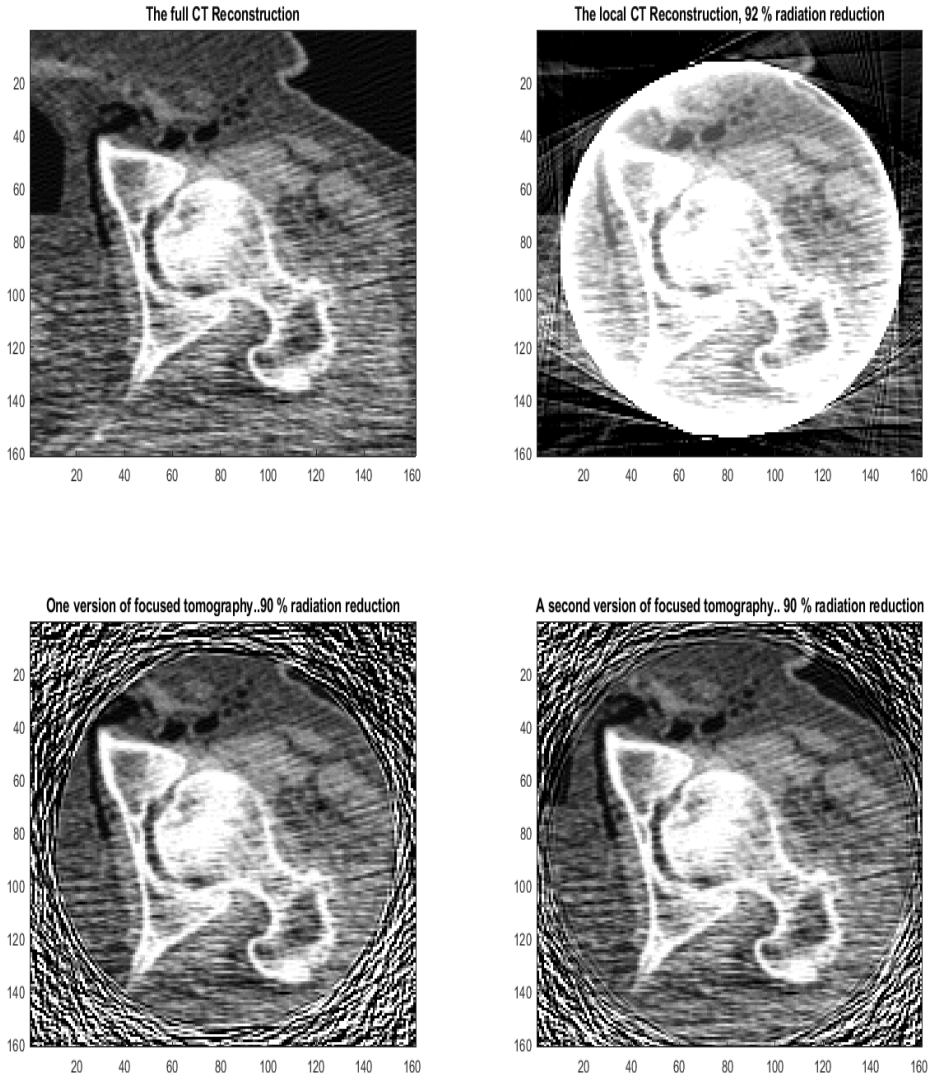

Figure 13: We illustrate the radiation exposure recommended for a central region and a non-central of an Spinal image similar to the schemes in [3, 4]. In these images we utilized off ROI radiation levels which were much lower than those of Figure 9. We illustrate closeups of the ROI above. This results in a radiation levels by approximately 85%. As opposed to the 0-1 sampling scheme in [3, 4], this adaptive sampling method was designed for arbitrary geometries, and can be implemented simply in a fan-beam geometry. The original non-noise related reconstruction is at top left, the reconstruction with totally local data is seen on the right. The bottom row shows the reduced radiation methods with FCT1 on the left, and FCT2 on the right.

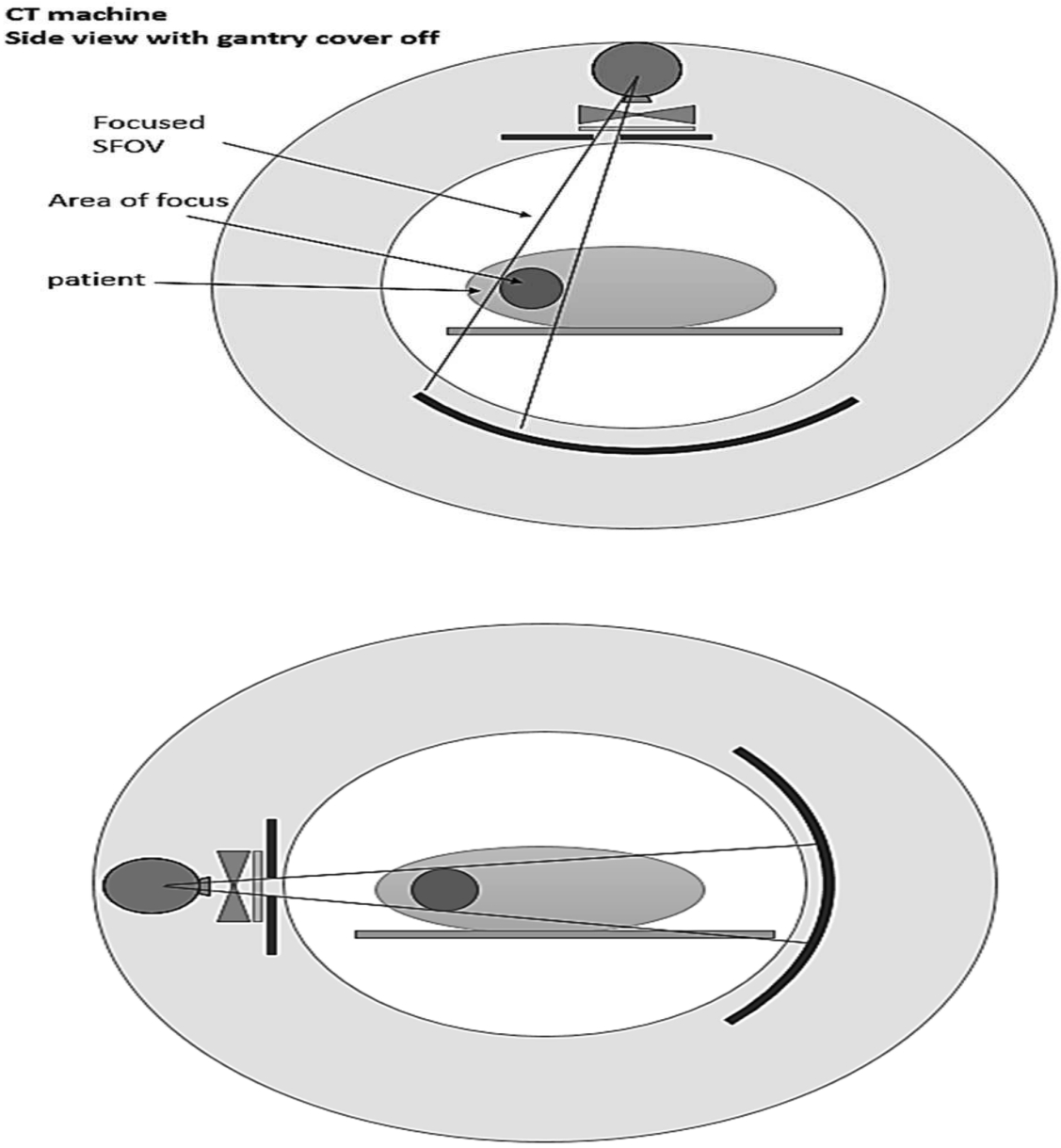

Figure 14: We illustrate the radiation exposure recommended for a central region and a non-central of an image similar to the schemes in [3, 4]. This results in a radiation levels by as much at least 85%. As opposed to the 0-1 sampling scheme in [3, 4], this adaptive sampling method was designed for arbitrary geometries, and an be implemented in a fan-beam geometry. The original non-noise related reconstruction is at top left, and a noisy reconstruction is at top left. The middle and bottom rows show the noisy reconstruction with full data on the left, and the reduced radiation reconstructions of a ROI on the right.

References

[1] NIH Announcement, "Decreasing Patient Radiation Dose from CT Imaging: Achieving Sub-mSv Studies (U01)".

[2] A. Faridani, E.L. Ritman, K.T. Smith, "Local Tomography", SIAM J. Applied Math, 1992.

[3] T.Olson, and J. DeStefano, "Wavelet localization of the Radon Transform", IEEE Signal Processing, 1994.

[4] T. Olson, "Optimal Time-Frequency Projections for Localized Tomography", Annals of Biomedical Engineering, 1995.

[5] D.M. Healy Jr., T. Olson, J.B. Weaver: "Reduced Motion Artifacts in Medical Imaging by Adaptive Spatio-Temporal Reconstruction," Numerical Algorithms 9:55-84 (1995).